

RESEARCH ARTICLE

A Low Molecular Weight Folate Receptor Targeted Contrast Agent for Magnetic Resonance Tumor Imaging

Tammy L. Kalber,¹ Nazila Kamaly,^{1,2} Po-Wah So,³ John A. Pugh,⁴ Josephine Bunch,⁴ Cameron W. McLeod,⁴ Michael R. Jorgensen,² Andrew D. Miller,² Jimmy D. Bell¹

¹Metabolic and Molecular Imaging Group, MRC Clinical Sciences Centre, Imperial College London, Hammersmith Hospital, London, W12 0NN, UK

²Imperial College Genetic Therapies Centre, Department of Chemistry, Imperial College London, Flowers Building, Armstrong Road, London, SW7 2AZ, UK

³Biological Imaging Centre, Imperial College London, Hammersmith Hospital, London, W12 0NN, UK

⁴Centre for Analytical Sciences, Department of Chemistry, University of Sheffield, Brook Hill, Sheffield, S3 7HF, UK

Abstract

Purpose: This study aims to develop a low molecular weight folate receptor (FR) contrast agent for MR tumor imaging.

Procedures: Gadolinium-tetraazacyclododecane tetraacetic acid (Gd.DOTA) was conjugated to folic acid to create Gd.DOTA.Folate. The efficacy of Gd.DOTA.Folate to bind FR was evaluated *in vitro* by inductively coupled mass spectrometry (ICP-MS) and *in vivo* by magnetic resonance imaging (MRI) tumor enhancement over 14 h, utilizing an overexpressing α -FR cell line (IGROV-1), compared to an α -FR-negative cell line (OVCAR-3). Gd.DOTA.Folate localization *ex vivo* was verified by laser ablation ICP-MS.

Results: ICP-MS confirmed Gd.DOTA.Folate uptake by IGROV-1 cells and competitive binding with free folic acid inhibited binding. IGROV-1 tumors showed an increase in R_1 at 2 h, which increased significantly over 14 h post-Gd.DOTA.Folate with clear enhancement on MR images. This was not observed in controls.

Conclusion: These data support the use of FR-targeted small molecular weight MRI contrast agents for tumor imaging *in vivo*.

Key words: Folate receptor targeting, Folate, MRI contrast agents, Low molecular weight contrast agents, Tumor MRI, Tumor imaging, Gadolinium contrast agents

Introduction

The development of targeted contrast agents for the detection, diagnosis, and therapy of tumors using non-invasive imaging systems has become highly desirable. Evaluation of specific biomarkers that are overexpressed by tumor cells may be used to enhance detection, provide accurate diagnosis, evaluate tumor stage, aggressiveness and resistance to chemotherapy, and therefore aid in the design

of personal patient therapeutic care. One such biomarker of interest is the vitamin folate (or folic acid), necessary for cell proliferation and maintenance of new cells especially during periods of rapid cell division, playing an important role in the synthesis of nucleotides and DNA replication [1]. Folate is an essential vitamin as cells are unable to synthesize it themselves and therefore internalize circulating folate from dietary sources via membrane folate transport systems, such as the reduced folate carrier (RFC) and the folate receptor (FR). RFCs have low affinity for folate but high affinity for the reduced forms of folate such as dihydrofolate, tetrahy-

drofolate, or methylene tetrahydrofolate [2]. On the other hand, FRs bind folate with high affinity but not its reduced forms [3]. The human membrane FR has three isoforms: α -isoform, β -isoform, and γ -isoform. The α - and β -isoforms belong to a family of membrane-anchored glycoproteins of which the α -isoform is overexpressed in many cancer types, particularly in epithelial ovarian and uterine carcinomas, with low expression in normal tissues [4–6]. The conjugation of imaging tracers or therapeutic moieties via the γ -carboxyl group of folic acid conserves molecular enantiomeric purity without apparent effects on ligand binding affinity to FR ($K_d = 1 \times 10^{-10}$ M) [7]. Thus, folate is a valuable ligand for the development of FR-targeted imaging tracers, providing tumor-targeted imaging.

Several approaches have been developed using various imaging methodologies as well as different imaging tracers. Folate has previously been conjugated to fluorescent molecules [8–11], a variety of radionuclides [12–20], and more recently magnetic resonance imaging (MRI) contrast agents [21–29]. Successful tumor FR targeting by radio-imaging has been reported in humans [20] as well as in preclinical tumor models. Although radio-imaging methodologies are very sensitive, they have limited anatomical resolution necessitating multiple imaging modalities. Therefore, MRI maybe a more favorable imaging technique as it provides excellent soft tissue contrast as well as anatomic resolution. Targeting using folic acid with MR-sensitive probes has so far consisted of compounds containing polymeric gadolinium (Gd) chelates either as low molecular weight compounds [28, 29], as polymers or dendrimers [21–23], or incorporated into liposomes or microemulsions [26, 27], or conjugation to iron oxide nanoparticles [24, 25].

In this study, folic acid was coupled to gadolinium-tetraazacyclododecane tetraacetic acid (Gd.DOTA), an existing FDA-approved clinical contrast agent used for MRI (Dotarem®), via a very short bis(aminoethyl)ethylene glycol linker to produce the novel compound Gd.DOTA.Folate (Scheme 1), a low molecular weight FR-targeted MRI contrast agent. Tumor cell binding and distribution of the new agent was assessed by MRI over a period of 14 h using an overexpressing α -FR (α -FR+) human ovarian carcinoma cell line (IGROV-1) *in vitro* and as subcutaneous xenografts *in vivo*. A non- α -FR-expressing (α -FR-) human ovarian carcinoma cell line (OVCAR-3) was used as the control cell line. Additionally, the distribution of the Gd.DOTA.Folate molecule was confirmed either by inductively coupled mass spectrometry (ICP-MS) *in vitro* or laser ablation ICP-MS (LA-ICP-MS) *ex vivo* and correlated to histology at 14 h after dosing.

Materials and Methods

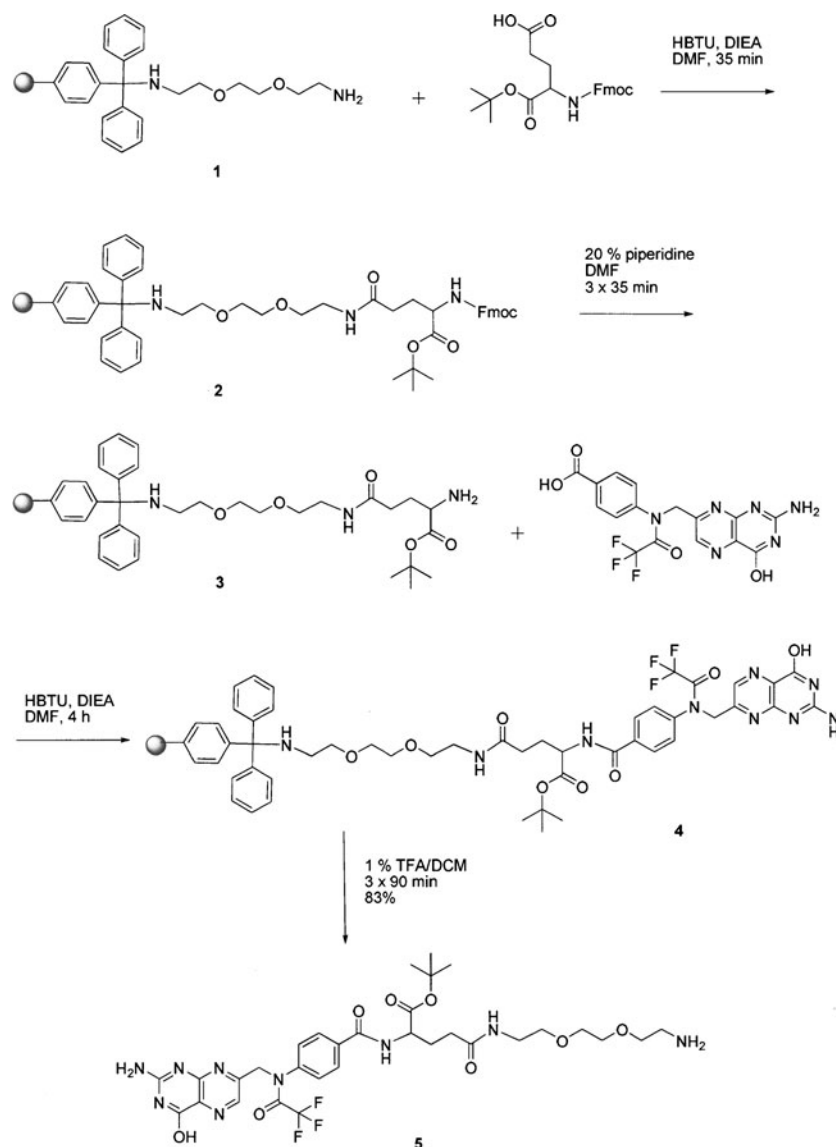
General Procedures

All reagents were purchased from Sigma-Aldrich (Dorset, UK), Macrocylics (Dallas, TX, USA), or Novabiochem (Darmstadt,

Germany) unless stated otherwise. Solvents were freshly distilled on appropriate driers and reactions run under a nitrogen atmosphere (CH_2Cl_2 was distilled over P_2O_5 , diisopropylethyl amine (DIEA) was distilled over NaOH). All compounds apart from those containing Gd were fully characterized by ^1H (400 MHz), ^{13}C (400 MHz) NMR spectroscopy (Bruker advance 400 spectrometer). Coupling constants J are given in hertz. The following abbreviations were used: s for singlet, d for doublet, t for triplet, q for quadruplet, and m for multiplet. Mass spectroscopy analyses were performed using VG-070B, Joel SX-102, or Bruker Esquire 3000 ESI instruments. Analytical HPLC was conducted on a Hitachi-LaChrom L-7150 pump system equipped with a Polymer Laboratories PL-ELS 1000 evaporative light scattering detector. Flash column chromatography was performed using Merck 0.040 to 0.063 mm, 230 to 400 mesh silica gel. Commercial compounds were used as received. All MRI experiments were conducted on a 4.7-T Varian Direct Drive MRI scanner (Varian Inc, Palo Alto, CA, USA). All procedures on animals were carried out in accordance with UK Home Office regulations and the Guidance for the Operation of Animals (Scientific Procedures) Act (1986).

Chemical Synthesis

4-{2-[2-(2-Amino-ethoxy)-ethoxy]-ethylcarbamoyl}-2-{4-[(2-amino-4-hydroxy-pteridin-7-ylmethyl)-(2,2,2-trifluoroacetyl)-amino]-benzoylamino}-Butyric Acid tert-Butyl Ester, 5 bis-(Aminoethyl) ethylene glycol resin (106.03 mg, 0.0816 mmol, 1.5 eq.) was added to a solid phase synthesis vessel and allowed to swell in CH_2Cl_2 while agitated overnight. The resin was washed with CH_2Cl_2 ($\times 3$), MeOH ($\times 3$), and DMF ($\times 3$) and coupled with (9-fluorenyl) methoxycarbonyl (Fmoc)-Glu(OtBu)-OH (104 mg, 0.816 mmol, 3 eq.) using *O*-benzyotriazol-1-yl- N,N,N' -tetramethyluronium hexafluorophosphate (HBTU; 3 eq.) and DIEA (5 eq.) in DMF (35 min). A chloranil test was performed to monitor the completion of the reaction, and coupling was repeated if necessary. The Fmoc protecting group was cleaved with 20% piperidine in DMF (3 min, $\times 3$). The resin was subsequently washed with MeOH and DMF ($\times 2$). The chloranil test was performed to monitor the reaction. N^{10} -(Trifluoroacetyl)pteroic acid (1.15 eq.) was added to the resin in addition to HBTU (3 eq.) and DIEA (5 eq.). To this was added DMF and the flask agitated for 4 h. The resin was washed with CH_2Cl_2 ($\times 3$), MeOH ($\times 3$), and DMF ($\times 3$) and cleaved from the product with 1% TFA/ CH_2Cl_2 (90 min, $\times 3$). The filtrate was collected and the solvent removed *in vacuo* to obtain amine 5. The crude product was purified with flash column chromatography and eluted with $\text{CH}_2\text{Cl}_2/\text{MeOH}/\text{H}_2\text{O}$ (77.3:20.5:2.2%) to yield a yellow oil (83%). ^1H NMR (400 MHz, MeOD) δ_{H} 8.70 (1H, s, $-\text{N}=\text{CH}-$), 7.92 (2H, d, J 8.8, aromatic), 7.59 (2H, d, J 8.4, aromatic), 5.19 (1H, s, $-\text{OH}$), 4.66 (1H, q, $-(\text{H}_3\text{C})_3\text{COOCC}-$), 4.12 (2H, q, $-\text{N}=\text{CCH}_2\text{N}-$), 3.64 (4H, m, $-\text{CH}_2\text{OCH}_2\text{CH}_2\text{OCH}_2-$), 3.52 (4H, m, $-\text{CH}_2\text{OCH}_2\text{CH}_2\text{OCH}_2-$), 3.41 (2H, m, $-\text{CONHCH}_2-$), 3.12 (2H, t, $-\text{H}_2\text{NCH}_2-$), 2.39 (2H, m, $t\text{-BuOCOCH}_2-$), 2.27 (2H, m, $t\text{-BuOCOCH}_2\text{CH}_2-$), 2.02 (2H, m, $-\text{CH}_2\text{NH}_2$), and 1.48 (9H, q, $t\text{-BuO}-$)ppm. ^{13}C NMR (400 MHz, MeOD) δ_{C} 175.32 ($-\text{C}-\text{OH}$), 171.00 ($-\text{COO}-$), 128.31 (C -aromatic), 129.80 (C -aromatic), 69.97 ($-\text{OCH}_2-$), 69.24 ($(\text{H}_3\text{C})_3\text{C}-$), 66.49



Scheme 1. Synthesis of folate coupled precursor.

($-\text{CONHCH}_2\text{CH}_2\text{O}-$), 60.00 ($-\text{OCH}_2\text{CH}_2\text{O}-$), 53.47 ($-\text{N}=\text{CCH}_2\text{N}-$), 39.27 ($-\text{CONHCH}_2-$), 38.84 (H_2NCH_2-), 33.95 ($-\text{COCHCH}_2-$), 31.87 ($-\text{COCHCH}_2\text{CH}_2-$), and 26.84 ($\text{H}_3\text{C}-\text{C}-$) ppm. HPLC: $t_R=12.95$ min, column C-4 peptide: gradient mix A=MeCN/0.1% TFA mix B= H_2O /TFA mix C=MeOH/ CHCl_3 mix D=MeOH, 0.0 min [100% B], 15–25.0 min [100% A], 25.1–45.0 min [100% D]; flow 1 mL/min. HRMS (FAB+) calculated for $\text{C}_{31}\text{H}_{40}\text{F}_3\text{N}_9\text{O}_8\text{m/z}$ 723.700, found 724.3033 (M^+).

2-{4-[(2-Amino-4-hydroxy-pteridin-7-ylmethyl)-amino]-benzoylamino}-4-[2-(2-{2-[2-(4,7,10-tris-carboxymethyl-1,4,7,10-tetraazacyclododec-1-yl)-acetylamino]-ethoxy}-ethoxy)-ethylcarbamoyl]-Butyric Acid, 6 Amine 5 (50 mg, 0.086 mmol) was added to an air evacuated flask followed by the addition of DOTA-NHS (62.2 mg,

0.0749 mmol) and triethylamine (31.3 μL , 0.225 mmol). The air was further displaced from the flask, and 40 mL of dry CH_2Cl_2 was added and the reaction stirred under vacuum at 40°C overnight. The solvents were removed *in vacuo* and the crude product was purified by column chromatography to yield a light yellow/orange solid (57%). ^1H NMR (400 MHz, MeOD/ CDCl_3 1:2v/v) δ_{H} 8.64 (1H, s, $-\text{N}=\text{CHC}-$), 7.90 (1H, d, J 8.8, H -aromatic), 7.49 (1H, d, J 8.4), 5.22 (1H, s, $-\text{OH}$), 4.59 (1H, s, $-\text{OOCCH}_2-$), 4.43 (2H, m, $-\text{N}=\text{CCH}_2-$), 3.50 (4H, m, $\text{H}_2\text{CH}_2\text{COCH}_2\text{CH}_2\text{OCH}_2-$), 3.38 (4H, m, $\text{H}_2\text{CH}_2\text{COCH}_2\text{-CH}_2\text{OCH}_2-$), 3.30 (8H, m, $4 \times \text{HOOCCH}_2$'s), 3.21 (4H, m, $-\text{CONHCH}_2$, and $-\text{H}_2\text{CNH-DOTA}$), 2.8 (16H, m, br, DOTA ring CH_2 's), 2.20 (4H, m, br, $-\text{CHCH}_2\text{CH}_2-$), and 1.47 (9H, $3 \times \text{H}_3\text{C}-$) ppm. ^{13}C NMR (400 MHz, MeOD/ CDCl_3 1:2v/v) δ_{C} 182.23 ($-\text{C}-\text{OH}$), 177.59 ($-\text{COOH}$), 177.13 ($-\text{NHCO-CH}_2\text{CH}_2$), 175.47 ($t\text{-BuCOOCH}_2-$), 172.30 ($-\text{C}=\text{CCO}-$), 132.85 (C -aromatic), 125.48 ($-\text{CF}_3$), 115.90 (C -aromatic), 73.86 ($t\text{-BuCOO}-$), 73.28, 72.81 (ethylene carbons), 63.13 ($-\text{COOCH}_2-$), 61.24, 60.87, 57.96, 55.96

($-\text{CH}_2$'s), 52.87–49.93 (DOTA CH_2 's), 31.47 ($-\text{CH}_3$), and 21.35 ($-\text{OOCCHCH}_2-$)ppm. HPLC $t_R=3.23$ min, column C-4 peptide: gradient mix A=MeCN/0.1% TFA mix B= H_2O /TFA mix C=MeOH/ CHCl_3 mix D=MeOH, 0.0 min [100% B], 15–25.0 min [100% A], 25.1–45.0 min [100% D]; flow 1 mL/min. MS (ESI+) calculated for $\text{C}_{47}\text{H}_{66}\text{F}_3\text{N}_{13}\text{O}_{15}m/z$ 1,110.100, found 1,111.30 (M+).

Gd.DOTA.Folate 7 A stoichiometric amount of DOTA.Folate 6 (41.7 mg, 0.038 mmol) and gadolinium chloride (12.96 mg, 0.038 mmol) was stirred in distilled water (15 mL) at 90°C for an overnight period. The water was removed by freeze-drying the solution to yield an orange crystalline solid. The xylenol orange assay did not reveal any free gadolinium ions, and the isotopic peaks of gadolinium were visible in the ESI MS trace. HPLC analysis $t_R=15.63$ min, column C-4 peptide: gradient mix A=MeCN/0.1% TFA mix B= H_2O /TFA mix C=MeOH/ CHCl_3 mix D=MeOH, 0.0 min (100% B), 15–25.0 min (100% A), 25.1–45.0 min (100% D); flow 1 mL/min. MS (ESI-) calculated for $\text{C}_{41}\text{H}_{56}\text{GdN}_{13}\text{O}_{14}m/z$ 1,112.212, found 1,111.50 (M-).

Xylenol Orange Test The presence of free gadolinium ions was determined by measuring the absorbance at 573 nm of a mixture of xylenol orange solution (990 μL , 0.5 mM in sodium acetate buffer (0.1 M, pH 5.2) and test solution (in an appropriate solvent) containing the gadolinium compound (10 μL). Extinction coefficient $\epsilon=20,700$ $\text{Lmol}^{-1}\text{cm}^{-1}$, whereby $[\text{free Gd}]=A573/\epsilon$.

Chloranil Test To 1–5 mg of resin was added one drop of 2% acetaldehyde in DMF (v/v) followed by one drop of 2% *p*-chloranil in DMF (w/v). The sample was allowed to stand at room temperature for 5 min. Blue-stained beads indicate the presence of secondary amines.

In Vitro

Relaxivity of MR Phantoms 0.5 mM Gd.DOTA.Folate, DOTA.Folate, Gd.DOTA (Dotarem, Guerbet, France), or water was used to assess T_1 relaxation. A range of concentrations (0.03–0.5 mM) of Gd.DOTA.Folate or Gd.DOTA was then used to calculate relaxivity (r_1) for each contrast agent. Phantoms were placed in a quadrature ^1H volume coil and positioned into the MRI scanner. A spin-echo sequence with the following parameters was used to assess T_1 : 10 TRs ranging from 50 to 7,000 ms, TE=10 ms, FOV=45×45 mm, averages 1, matrix size 256×128, and a 2.0 mm thickness.

Tissue Culture Human ovarian carcinoma IGROV-1 and OVCAR-3 were grown in 10% heat inactivated fetal calf serum (Invitrogen, Paisley, UK) supplemented Dulbecco's modified Eagles media (Sigma) in T175 flasks (Fisher Scientific, Loughborough, UK) at 37°C in a humidified atmosphere containing 95% air and 5% CO_2 .

Cells were then modified to grow in folate-free RPMI-1640 media (Invitrogen), supplemented with 10% heat inactivated fetal calf serum for approximately 5 days prior to cell experiments or *in vivo* inoculation. Previously we have shown that the IGROV-1 cells overexpress the α -FR isoform by FACS analysis, compared to OVCAR-3 and HeLa human ovarian carcinoma cell lines [27], consistent with that previously reported by Corona *et al.* [30]. As the OVCAR-3 cell line showed minimal α -FR expression in our hands, this cell line was used as a negative control to assess excess binding of Gd.DOTA.Folate in our *in vitro* and *in vivo* imaging studies.

Gd.DOTA.Folate Cellular Uptake by MRI and ICP-MS IGROV-1 or OVCAR-3 cells were plated at 1.5×10^5 in T25 flasks 24 h prior to incubation of 0.5 mM Gd.DOTA.Folate, DOTA.Folate, Gd.DOTA, or water (compounds were dissolved in sterile water as a 1-mM stock solution and then made to 0.5 mM by dilution with serum-free, folate-free media). For MRI, cells were washed with PBS, harvested, and pelleted at 2, 8, and 14 h after incubation. The cell pellets were re-suspended in 1 mL PBS and the numbers of viable and non-viable cells counted with trypan blue solution (Sigma, UK) to calculate percentage viability. The cells were then pelleted again and re-suspended in 1% agarose (Sigma, UK) and scanned as described for phantoms. For ICP-MS, cells were washed, harvested, and pelleted as before after 1 h. The cells were washed with PBS and then lysed using 300 μL TRIzol (Invitrogen) and then made up to 7.5 mL with water containing 2% concentrated nitric acid (VWR, Leicestershire, UK). Samples were then run in triplicate on a Varian ICP-MS (Varian Inc.). For ICP-MS samples, competitive binding with free folic acid was also carried out to assess whether Gd.DOTA.Folate uptake was due to FR binding. For these samples, an excess of 1 mM folic acid (Sigma) was added 15 min prior to the addition of 0.5 mM Gd.DOTA.Folate, DOTA.Folate, Gd.DOTA, or water. After 1 h, the cells were washed, harvested, and processed as before for ICP-MS.

In Vivo

Tumor Induction and MRI IGROV-1 or OVCAR-3 cells of 5×10^6 /0.1 mL were inoculated into the flank of 6–8-week-old Balb/c nude mice (Harlan, UK). Once palpable, tumors were measured in three orthogonal dimensions every 2 days using calipers. Tumor volumes were estimated assuming an ellipsoid shape using the formula volume = length × width × depth × $\pi/6$. When tumors reached approximately 7–10 mm in diameter, mice were anesthetized with an isoflurane/ O_2 mix and scanned as described for phantoms with the use of a warm air blower to maintain the body core temperature at 37°C, using the parameters: TRs=400, 700, and 2,800 ms; TE=15 ms, FOV=45×45 cm, one average, and matrix size=256×128. Twenty contiguous 2-mm-thick transverse slices covering the whole abdomen. Mice were removed from the scanner and a single intravenous 200- μL bolus injection of 1 mM Gd.DOTA.Folate ($n=3$ for both IGROV-1 and OVCAR-3 tumor xenografts) or 1 mM Gd.DOTA ($n=3$ for both IGROV-1 and OVCAR-3 tumor xenografts) was administered via the tail vein. Mice were then re-scanned with the same parameters at 2 and 14 h post-administration. After the final scan, mice were sacrificed and the tumor was excised and frozen for LA-ICP-MS and hematoxylin and eosin

(H&E) staining. The liver and kidney were also taken but for H&E only.

MRI Data Analysis A region of interest (ROI) was drawn around the whole tumor excluding the skin in MR images using Image J (National Institute of Health, USA) [31]. Mean signal intensities of the ROIs at different TR values were measured and used to calculate the MR longitudinal relaxation time T_1 and relaxation rate R_1 ($R_1=1/T_1$) values using Prism™ (Graphpad, San Diego, CA, USA). Mean T_1 and R_1 values for each cohort were derived, and a two-tailed unpaired t test assuming equal variances was performed at each time point to determine significant difference, at the 5% level statistical significance. Signal intensities were also recorded from circular ROIs drawn in the liver and kidney to assess clearance, and T_1 and R_1 were calculated (as above).

LA-ICP-MS Frozen tumor tissue was mounted onto a cryostat chuck using water/ice slush frozen to -20°C and 20 μm sections cut using a cryotome. The laser ablation system (LSX-200, Cetac, 266 nm Nd:YAG) was configured to perform multiple line rasters, to generate 2D elemental distribution maps. A beam diameter of 50 μm was used for ablating sections (energy 0.6 mJ), a scanning speed of 50 $\mu\text{m/s}$, and laser frequency of 10 Hz. For ICP-MS (Agilent, HP4500 Series 100), the elements Gd¹⁵⁷ and Zn⁶⁶ (an element widespread in biochemistry) were measured in a time-resolved mode, and the isotopes were selected on the basis of high-percentage abundance and minimal isobaric and polyatomic interferences. Tumor sample areas were in the range 130–190 mm^2 . Elemental maps were produced using the Graphis software package (Kylebank Software Ltd, Ayr, UK). Adjacent sections were taken for H&E staining.

Histological Assessment Sections were incubated with hematoxylin solution for 1 min and then in freshly prepared eosin Y (both Sigma) for 30 s. The sections were then dehydrated with alcohol and passed through histoclear (Fisher Scientific), mounted with DPX (VWR), and imaged using an Olympus IX71 microscope (Olympus, Middlesex, UK).

Results

Synthesis of Gd.DOTA.Folate

Solid phase synthesis was utilized for the synthesis of folate precursor **5** (Scheme 1). Firstly, an orthogonally protected glutamic acid precursor was coupled to the bis-(aminoethyl) ethylene glycol trityl resin **1** using HBTU and DIEA. Deprotection of the Fmoc group yielded compound **3** which was subsequently coupled with *N*-(trifluoroacetyl) pteric acid to give the resin bound product **4**. A facile mildly acidic resin cleavage afforded the folate coupled amino precursor **5**. Precursor **5** was then reacted with the activated DOTA-NHS ester to provide the folate.DOTA ligand **6** (Scheme 2). This compound was analyzed by both ¹H and ¹³C NMR. A stoichiometric addition of gadolinium chloride to **6** resulted

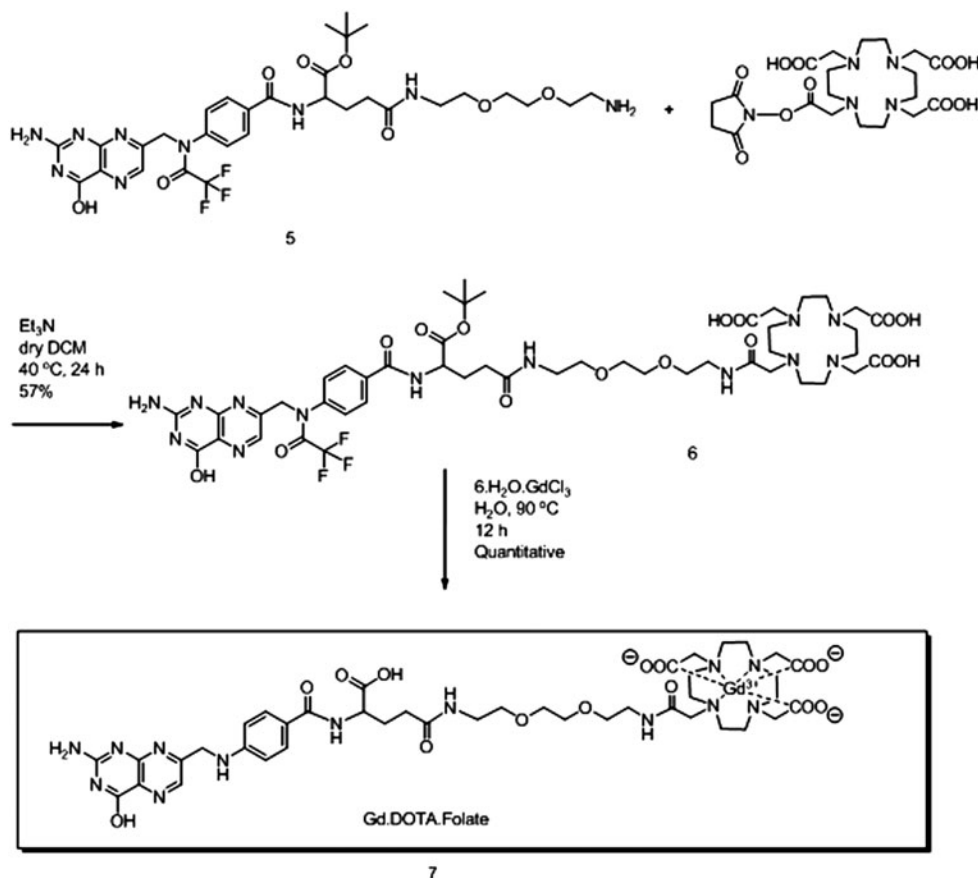
in our target molecule Gd.DOTA.Folate **7**. Interestingly, both the tertiary butyl and trifluoroacetyl protecting groups of compound **6** were also removed in this final step due to the acidity produced by HCl formation during the Gd chelating step (Scheme 2). Gd.DOTA.Folate **7** was assessed for its purity by HPLC and analyzed by mass spectrometry, where the isotopic Gd peaks were clearly visible. The xylenol orange assay did not indicate the presence of free Gd ions to any significant degree.

MR Relaxivity of Gd.DOTA.Folate

The MRI efficacy of Gd.DOTA.Folate **7** in aqueous solution was measured, and a 70% reduction in the bulk water T_1 value was observed compared to water alone and DOTA.Folate control solutions. Additionally, the r_1 relaxivity for Gd.DOTA.Folate was calculated to be $1.28 \text{ mM}^{-1} \text{ s}^{-1}$, slightly lower than that of the non-conjugated Gd.DOTA ($3.66 \text{ mM}^{-1} \text{ s}^{-1}$).

Gd.DOTA.Folate Cellular Uptake by MRI and ICP-MS

Trypan blue staining of IGROV-1 and OVCAR-3 cells at 2, 8, and 14 h time points after incubation with 0.5 mM of Gd.DOTA.Folate, DOTA.Folate, or Gd.DOTA showed no significant differences in the number of viable cells counted compared to controls. This suggests that the conjugation product of folic acid and Gd.DOTA is essentially non-toxic to cells. Analysis of MR images obtained from cell pellets at these times after incubation did not show any signal enhancement or changes in R_1 for either compound compared to control cells for either cell line. However, ICP-MS results of cell pellets after 1 h showed that gadolinium was detectable in both IGROV-1 and OVCAR-3 cell pellets incubated with 0.5 mM Gd.DOTA.Folate compared to controls. The α -FR+ IGROV-1 cells, presented a significantly higher concentration of gadolinium which was approximately double that presented by the α -FR- OVCAR-3 cells (Fig. 1). The competitive binding experiments with free folic acid showed that the concentration of gadolinium within the IGROV-1 cells was significantly reduced ($p < 0.01$). OVCAR-3 cells also showed a reduction in gadolinium uptake although not to the same extent (Fig. 1). As we have previously determined the OVCAR-3 cell line to be α -FR negative by immunohistochemistry experiments, the uptake observed by the OVCAR-3 cell line may suggest that folic acid is taken up via non-FR-mediated mechanisms [27]. However, free folic acid did not give complete inhibition in either cell line suggesting that another mechanism of uptake is also taking place in both cell lines. Nonetheless, the two-fold increased uptake for Gd.DOTA.Folate in the IGROV-1 cell line suggests that there is an increased uptake of folic acid in this cell line that is



Scheme 2. Synthesis of Gd.DOTA.Folate.

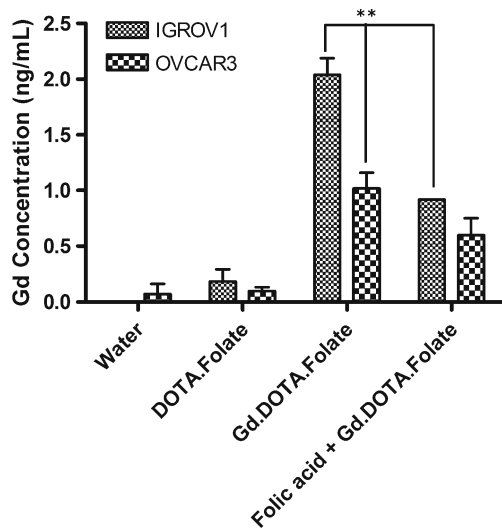


Fig. 1. Gadolinium concentration as evaluated by ICP-MS of OVCAR-3 and IGROV-1 incubated with either 0.5 mM DOTA.Folate, Gd.DOTA.Folate, or Gd.DOTA.Folate in competition with previous incubation of 1-mM free folic acid. Data points are mean \pm standard deviation. $**P \leq 0.01$ IGROV-1 + Gd.DOTA.Folate compared to both OVCAR-3 + Gd.DOTA.Folate and IGROV-1 + Folic acid + Gd.DOTA.Folate.

due to the overexpression of α -FR which may be sufficient for the purposes of *in vivo* tumor MRI.

In Vivo Tumor MRI

MR images showed clear tumor enhancement within the α -FR+ IGROV-1 tumor xenograft at both the 2 and 14 h time point post-administration of Gd.DOTA.Folate, compared to the baseline image (Fig. 2a), whereas the α -FR- OVCAR-3 tumor xenografts did not appear to show any tumor enhancement for Gd.DOTA.Folate on the images (Fig. 2b). This was also reflected in the R_1 values. An increase in R_1 was observed at 2 h in the IGROV-1 tumors treated with Gd.DOTA.Folate which further increased and became significant ($p < 0.05$) at the 14 h time point (Fig. 3). No other change in R_1 was noted in any of the other groups (Fig. 3). Although the increase at the 2 h time point is not significant, there appears to be a definite increase in R_1 compared to the Gd.DOTA control IGROV-1 group as well as both Gd.DOTA.Folate and Gd.DOTA OVCAR-3 groups. The non-conjugated control Gd.DOTA does not appear to be evident within either tumor even at the earliest 2 h time point, which is consistent with a non-targeted agent of low molecular weight, which is rapidly cleared from the blood and excreted by the kidney.

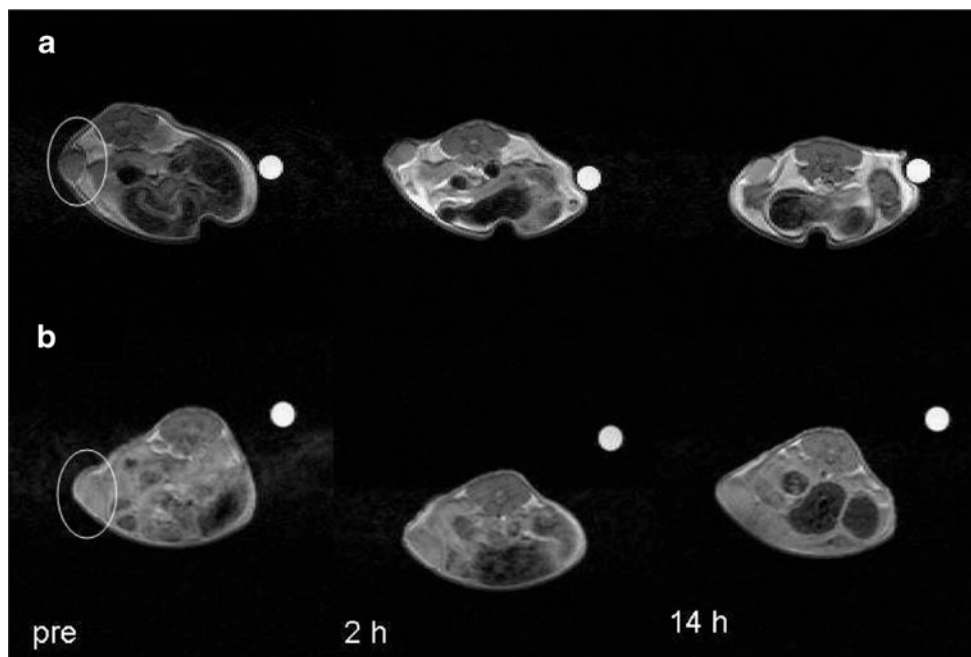


Fig. 2. MR images showing clear tumor enhancement within the α -FR+ IGROV-1 tumor xenograft (a) and the α -FR- OVCAR-3 tumor xenografts not showing any tumor enhancement for Gd.DOTA.Folate (b).

Therefore, the gradual increase in R_1 over the 14 h in the Gd.DOTA.Folate-treated IGROV-1 group suggests that the compound is not washed out of the tumor over this time period, and consequently, the compound must either be bound to receptors or have been internalized into the endosomes within the tumor cells, through receptor-mediated transportation [32]. As the α -FR- OVCAR-3 tumors showed no uptake, these *in vivo* results therefore confirm that accumulation of Gd.DOTA.Folate in these ovarian tumors requires the expression of the FR.

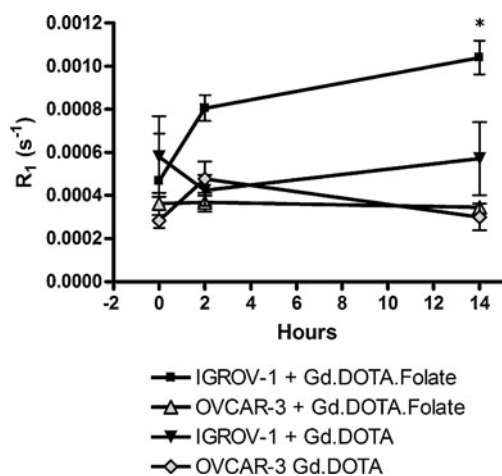


Fig. 3. IGROV-1 and OVCAR-3 whole tumor assessment of changes in R_1 (per second) measured pre-, 2, and 14 h post-injection of 200 μ l of 1 mM Gd.DOTA.Folate or Gd.DOTA. Data points are mean \pm standard deviation. * $P \leq 0.05$ IGROV-1 + Gd.DOTA.Folate at 14 h compared to baseline.

When the liver and kidneys were assessed by MR, both organs showed a slight increase in the mean R_1 (data not shown). However, these results were not significant and were not consistently shown to be enhanced on MR images and in all animals. This suggests that there was a low concentration of binding of Gd.DOTA.Folate to these organs compared to that of tumor tissue.

LA-ICP-MS

The presence of gadolinium within tumors was assessed at the 14 h time point by LA-ICP-MS. Elemental maps confirmed the presence of Gd¹⁵⁷ consistent with the increased signal enhancement and increased R_1 in the IGROV-1 tumors administered with Gd.DOTA.Folate (Fig. 4c). Gadolinium was mainly situated in the rim of the tumor, shown to be the areas of highly vascularized viable tumor tissue by co-localization of Zn⁶⁶ (found in viable biological tissue; Fig. 4b) with H&E staining (Fig. 4a). No Gd¹⁵⁷ was detected in the necrotic areas of the tumor core or in tumors from mice injected with the control gadolinium-free agent, DOTA.Folate (Fig. 4d).

Discussion

In this study, an MR visible imaging tracer that was targeted to FR has been synthesized by the conjugation of Gd.DOTA with folic acid via a bis(aminoethyl)ethylene glycol linker to produce the compound Gd.DOTA.Folate. The effectiveness of Gd.DOTA.Folate to bind to FR was assessed in the α -FR overexpressing IGROV-1 cell line compared to the non- α -

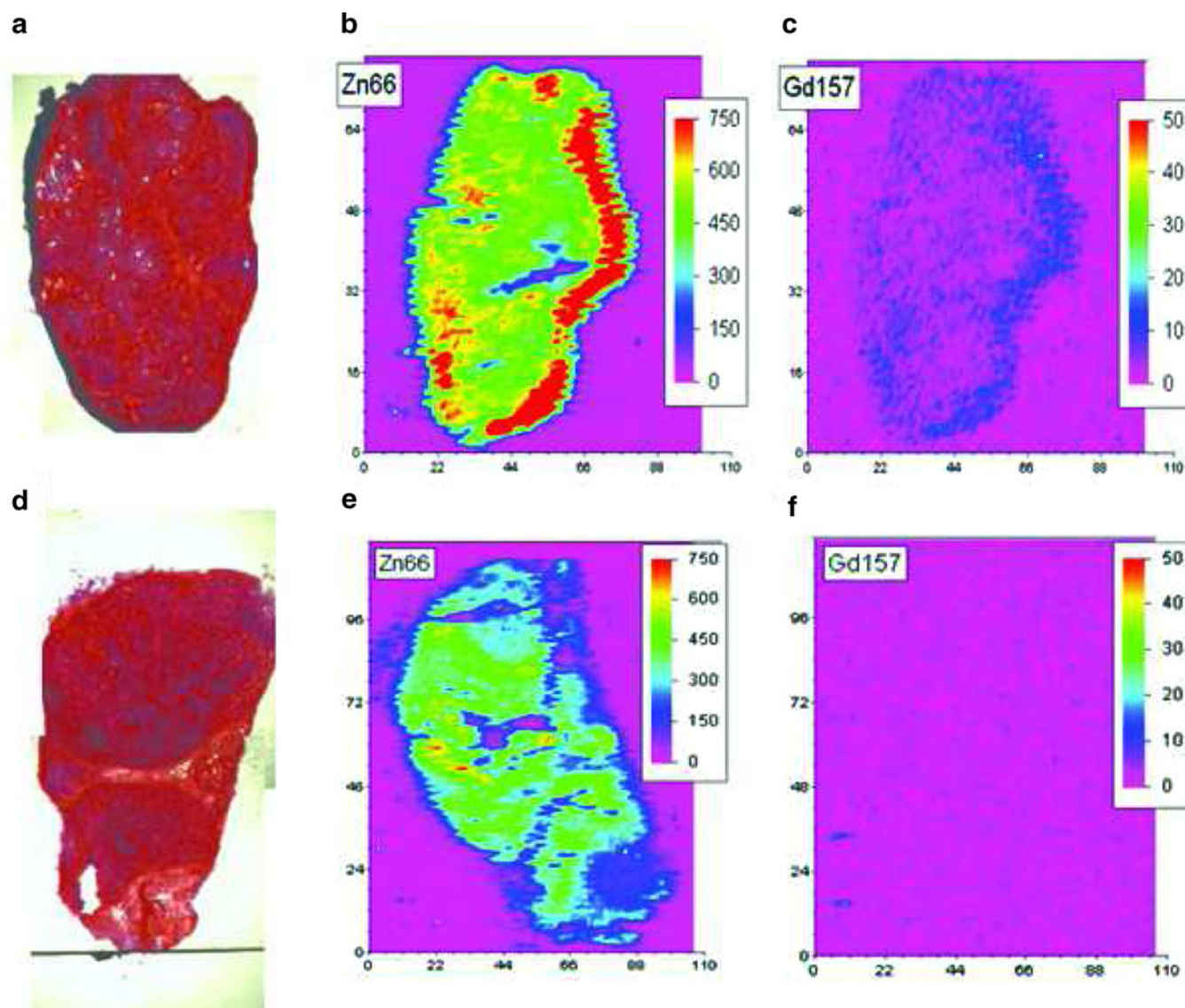


Fig. 4. H & E Stained sections (a & d) and LA-ICP-MS element maps of Zn⁶⁶ and Gd¹⁵⁷ distribution in IGROV-1 tumours 14 h after administration of either 200 µl 1 mM Gd.DOTA.Folate (a, b & c) or DOTA.Folate (d, e & f).

FR-expressing OVCAR-3 ovarian carcinoma cell line *in vitro* and *in vivo* using solid tumor xenografts. MR images were taken of both cell pellets after incubation with, or of *in vivo* tumors at longitudinal time points after administration of, Gd.DOTA.Folate or controls. R_1 values were calculated to assess accumulation of the paramagnetic material in the cells and tumors. R_1 values of cell pellets after incubation with Gd.DOTA.Folate did not result in significant changes in R_1 in either cell line (data not shown). In contrast, *in vitro* ICP-MS (Fig. 1), *in vivo* MRI, and *ex vivo* LA-ICP-MS data (Figs. 2, 3, and 4) do suggest that FR facilitate accumulation of Gd.DOTA.Folate

That the *in vitro* MR data do not appear to support the *in vivo* findings is surprising. However, others have also reported similar discrepancies when comparing *in vitro* and *in vivo* results using folate-targeted agents. *In vitro* work with both the ¹⁵³Gd-Folate dendrimer [33] and the P866 low molecular weight dimeric Gd.DOTA [29, 34]

shows these inconsistencies, suggesting potential sensitivity limitation *in vitro*, perhaps due to significant cellular variability in FR expression [34, 35]. Studies by Miotti *et al.* showed that although α -FR was the fundamental mechanism in folate internalization, the degree of folate internalized was not completely proportional to α -FR expression, as low α -FR-expressing cell lines were still capable of low levels of uptake [35]. The ICP-MS data in this study appear to support this, as although the α -FR+ IGROV-1 cell line presented a much higher degree of Gd.DOTA.Folate internalization than controls, there was still a degree of uptake within the latter. Furthermore, after competitive binding with free folic acid prior to incubation, although there was a significant decrease in the α -FR+ IGROV-1 cell line, the inhibition was not complete leaving a low level of Gd.DOTA.Folate uptake. Similar results have been reported in other studies

accessing binding in the presence of free folate suggesting the reduced folate carrier [28, 29, 35]. As the FR has a low affinity for folate but high affinity for the reduced forms of folate, there is a possibility that there is some degree of degradation of the folate end when in media/solution and that this is what is causing the non-FR-mediated uptake seen in α -FR- cells (OVCAR-3).

In contrast to the *in vitro* R_1 , *in vivo* tumor xenograft R_1 data are highly promising. In comparison with controls, there was a significant MR enhancement of the tumor as well as an increase in the R_1 values of IGROV-1 (FR-positive) tumors treated with Gd.DOTA.Folate at 2 h post-administration. This increased further at 14 h, showing clear benefits for MRI T_1 -weighted contrast imaging. Critically, the corresponding OVCAR-3 (FR-negative) tumors showed no enhancement or changes in R_1 suggesting that the beneficial MR enhancement and change in R_1 is mediated by the overexpression of α -FR in the IGROV-1 cell line. Gd.DOTA.Folate therefore demonstrates FR-mediated uptake into cancerous lesions *in vivo* in accordance with observations made with other FR-targeted contrast systems [28, 29, 36].

As the molecule is of low molecular weight, it is expected to be rapidly cleared as is the case with P866 [28, 29] and therefore should not benefit from the enhanced permeability and retention mechanism that can assist the tumor accumulation of other larger nanoparticle MRI contrast imaging systems [21–25, 27, 33]. However, Gd.DOTA.Folate demonstrates clear signs of accumulation leading to enhanced contrast over at least 14 h, and the presence of gadolinium was confirmed at the 14 h time point by LA-ICP-MS. It is expected that after internalization of Gd.DOTA.Folate into the endosome that the receptors are recycled into the plasma membrane. However, due to the rapid clearance of Gd.DOTA.Folate, we would expect that once the FRs are saturated, this would result in no further binding. This may therefore be explained by either prolonged binding and/or internalization into the cell, where it may then bind to intracellular proteins. These processes may therefore effectively slow the tumbling rate and increase the magnetic moment of the conjugate, affecting its relaxivity and therefore increase R_1 . However, recent studies have shown that activated macrophages also express FR- β [37] and that these macrophages can be targeted and followed using folate conjugates in models of inflammatory diseases such as rheumatoid arthritis, atherosclerosis as well as an IGROV-1 ovarian ascites tumor model [38–40]. Since tumor tissue generally presents an inflammatory microenvironment, it is therefore conceivable that the increase in signal may also be due to the accumulation of circulating activated macrophages that have been targeted by Gd.DOTA.Folate over the 14 h. This mechanism is also supported by the slight but non-significant change in R_1 identified in the liver over the same time period. This therefore suggests that folate-targeting with MR contrast agents have many variables.

In conclusion, a low molecular weight contrast agent Gd.DOTA.Folate was designed and synthesized that is capable of binding to FR-expressing tumors *in vivo*, increasing R_1 at both 2 and 14 h after administration, with clear enhancement on T_1 -weighted MR images. These observations suggest that small molecule targeted MRI contrast agents can be developed for the imaging of cancerous lesions and could be useful components to larger molecular/nanoparticle folate-targeted MRI contrast imaging systems that have recently been reported.

Acknowledgment. Funding for Tammy Kalber was provided by the MRC. The GTC is supported by EPSRC grant and is grateful for recent support from ImuThes Limited. The authors would also like to thank Mahamoud O. Hussein for his contribution to the chemical synthesis as well as Catherin Unsworth and Stanislav Strekopytov from the Department of Mineralogy at the Natural History Museum London for their expertise in running ICP-MS of the samples.

Conflict of Interest Disclosure. The authors declare that they have no conflict of interest.

References

1. Lucock M (2000) Folic acid: nutritional biochemistry, molecular biology, and role in disease processes. *Mol Genet Metab* 71:121–138
2. Matherly LH, Goldman DI (2003) Membrane transport of folates. *Vitam Horm* 66:403–456
3. Antony AC (1996) Folate receptors. *Annu Rev Nutr* 16:501–521
4. Campbell IG, Jones TA, Foulkes WD, Trowsdale J (1991) Folate-binding protein is a marker for ovarian cancer. *Cancer Res* 51:5329–5338
5. Coney LR, Tomassetti A, Carayannopoulos L et al (1991) Cloning of a tumor-associated antigen: MOV18 and MOV19 antibodies recognize a folate-binding protein. *Cancer Res* 51:6125–6132
6. Ross JF, Chaudhuri PK, Ratnam M (1994) Differential regulation of folate receptor isoforms in normal and malignant tissues *in vivo* and in established cell lines. Physiologic and clinical implications. *Cancer* 73:2432–2443
7. Luo JSM, Lantrip DA, Wang S, Fuchs PL (1997) Efficient synthesis of pyrofolic acid and pteroyl azide reagents for the production of carboxyl-differentiated derivatives of folic acid. *J Am Chem Soc* 119:10004–10013
8. Moon WK, Lin Y, O'Loughlin T et al (2003) Enhanced tumor detection using a folate receptor-targeted near-infrared fluorochrome conjugate. *Bioconjug Chem* 14:539–545
9. Kennedy MD, Jallad KN, Thompson DH, Ben-Amotz D, Low PS (2003) Optical imaging of metastatic tumors using a folate-targeted fluorescent probe. *J Biomed Opt* 8:636–641
10. Chen WT, Khazaie K, Zhang G, Weissleder R, Tung CH (2005) Detection of dysplastic intestinal adenomas using a fluorescent folate imaging probe. *Mol Imaging* 4:67–74
11. Kim IB, Shin H, Garcia AJ, Bunz UH (2007) Use of a folate-PPE conjugate to image cancer cells *in vitro*. *Bioconjug Chem* 18:815–820
12. Mathias CJ, Wang S, Waters DJ, Turek JJ, Low PS, Green MA (1998) Indium-111-DTPA-folate as a potential folate-receptor-targeted radiopharmaceutical. *J Nucl Med* 39:1579–1585
13. Guo W, Hinkle GH, Lee RJ (1999) ^{99m}Tc -HYNIC-folate: a novel receptor-based targeted radiopharmaceutical for tumor imaging. *J Nucl Med* 40:1563–1569
14. Leamon CP, Parker MA, Vlahov IR et al (2002) Synthesis and biological evaluation of EC20: a new folate-derived, (^{99m}Tc)-based radiopharmaceutical. *Bioconjug Chem* 13:1200–1210
15. Reddy JA, Xu LC, Parker N, Vetzal M, Leamon CP (2004) Preclinical evaluation of (^{99m}Tc)-EC20 for imaging folate receptor-positive tumors. *J Nucl Med* 45:857–866
16. Ke CY, Mathias CJ, Green MA (2005) Targeting the tumor-associated folate receptor with an ^{111}In -DTPA conjugate of pteric acid. *J Am Chem Soc* 127:7421–7426

17. Bettio A, Honer M, Muller C et al (2006) Synthesis and preclinical evaluation of a folic acid derivative labeled with ^{18}F for PET imaging of folate receptor-positive tumors. *J Nucl Med* 47:1153–1160
18. Muller C, Hohn A, Schubiger PA, Schibli R (2006) Preclinical evaluation of novel organometallic $^{99\text{m}}\text{Tc}$ -folate and $^{99\text{m}}\text{Tc}$ -pterolate radiotracers for folate receptor-positive tumour targeting. *Eur J Nucl Med Mol Imaging* 33:1007–1016
19. Okarvi SM, Jammaz IA (2006) Preparation and *in vitro* and *in vivo* evaluation of technetium- $^{99\text{m}}$ -labeled folate and methotrexate conjugates as tumor imaging agents. *Cancer Biother Radiopharm* 21:49–60
20. Siegel BA, Dehdashti F, Mutch DG et al (2003) Evaluation of ^{111}In -DTPA-folate as a receptor-targeted diagnostic agent for ovarian cancer: initial clinical results. *J Nucl Med* 44:700–707
21. Wiener EC, Konda S, Shadron A, Brechbiel M, Gansow O (1997) Targeting dendrimer-chelates to tumors and tumor cells expressing the high-affinity folate receptor. *Invest Radiol* 32:748–754
22. Konda SD, Aref M, Brechbiel M, Wiener EC (2000) Development of a tumor-targeting MR contrast agent using the high-affinity folate receptor: work in progress. *Invest Radiol* 35:50–57
23. Konda SD, Wang S, Brechbiel M, Wiener EC (2002) Biodistribution of a ^{153}Gd -folate dendrimer, generation=4, in mice with folate-receptor positive and negative ovarian tumor xenografts. *Invest Radiol* 37:199–204
24. Choi H, Choi SR, Zhou R, Kung HF, Chen IW (2004) Iron oxide nanoparticles as magnetic resonance contrast agent for tumor imaging via folate receptor-targeted delivery. *Acad Radiol* 11:996–1004
25. Sonvico F, Mornet S, Vasseur S et al (2005) Folate-conjugated iron oxide nanoparticles for solid tumor targeting as potential specific magnetic hyperthermia mediators: synthesis, physicochemical characterization, and *in vitro* experiments. *Bioconjug Chem* 16:1181–1188
26. Oyewumi MO, Mumper RJ (2002) Engineering tumor-targeted gadolinium hexanedione nanoparticles for potential application in neutron capture therapy. *Bioconjug Chem* 13:1328–1335
27. Kamaly N, Kalber T, Thanou M, Bell JD, Miller AD (2009) Folate receptor targeted bimodal liposomes for tumor magnetic resonance imaging. *Bioconjug Chem* 20:648–655
28. Corot C, Robert P, Lancelot E et al (2008) Tumor imaging using P866, a high-relaxivity gadolinium chelate designed for folate receptor targeting. *Magn Reson Med* 60:1337–1346
29. Wang ZJ, Boddington S, Wendland M, Meier R, Corot C, Daldrup-Link H (2008) MR imaging of ovarian tumors using folate-receptor-targeted contrast agents. *Pediatr Radiol* 38:529–537
30. Corona G, Giannini F, Fabris M, Toffoli G, Boiocchi M (1998) Role of folate receptor and reduced folate carrier in the transport of 5-methyltetrahydrofolic acid in human ovarian carcinoma cells. *Int J Cancer* 75:125–133
31. Rasband WS (1997–2008) ImageJ. U. S. National Institutes of Health, Bethesda. <http://rsb.info.nih.gov/ij/>
32. Terreno E, Geninatti Crich S, Belfiore S et al (2006) Effect of the intracellular localization of a Gd-based imaging probe on the relaxation enhancement of water protons. *Magn Reson Med* 55:491–497
33. Konda SD, Aref M, Wang S, Brechbiel M, Wiener EC (2001) Specific targeting of folate-dendrimer MRI contrast agents to the high affinity folate receptor expressed in ovarian tumor xenografts. *Magma* 12:104–113
34. McHugh M, Cheng YC (1979) Demonstration of a high affinity folate binder in human cell membranes and its characterization in cultured human KB cells. *J Biol Chem* 254:11312–11318
35. Miotti S, Bagnoli M, Ottone F, Tomassetti A, Colnaghi MI, Canevari S (1997) Simultaneous activity of two different mechanisms of folate transport in ovarian carcinoma cell lines. *J Cell Biochem* 65:479–491
36. Paulos CM, Reddy JA, Leamon CP, Turk MJ, Low PS (2004) Ligand binding and kinetics of folate receptor recycling *in vivo*: impact on receptor-mediated drug delivery. *Mol Pharmacol* 66:1406–1414
37. Nakashima-Matsushita N, Tomma T, Yu S et al (1999) Selective expression of folate receptor-beta and its possible role in methotrexate transport in synovial macrophages from patients with rheumatoid arthritis. *Arthritis Rheum* 42:1609–1616
38. Turk MJ, Breur GJ, Widmer WR et al (2002) Folate-targeted imaging of activated macrophages in rats with adjuvant-induced arthritis. *Arthritis Reum* 46:1947–1955
39. Turk MJ, Waters DJ, Low PS (2004) Folate-conjugated liposomes preferentially target macrophages associated with ovarian carcinoma. *Cancer Lett* 213:165–172
40. Ayala-Lopez W, Xia W, Varghese B, Low PS (2010) Imaging of atherosclerosis in apolipoprotein E knockout mice: targeting of a folate-conjugated radiopharmaceutical to activated macrophages. *J Nuc Med* 51:768–774